Myosin Va Becomes a Low Duty Ratio Motor in the Inhibited Form*

Osamu Sato, Xiang-dong Li, and Mitsuo Ikebe[1]

From the Department of Physiology, University of Massachusetts Medical School, Worcester, Massachueetts 01655

Vertebrate myosin Va is a typical processive motor with high duty ratio. Recent studies have revealed that the actin-activated ATPase activity of the full-length myosin Va (M5aFull) is inhibited at a low [Ca^{2+}], which is due to the formation of a folded conformation of M5aFull. To clarify the underlying inhibitory mechanism, we analyzed the actin-activated ATP hydrolysis mechanism of the M5aFull at the inhibited and the activated states, respectively. Marked differences were found in the hydrolysis, P$_i$ release, and ADP release steps between the activated and the inhibited states. The kinetic constants of these steps of the activated state were similar to those of the unregulated S1 construct, in which the rate-limiting step was the ADP release step. On the other hand, the P$_i$ release rate from acto-M5aFull was decreased in EGTA by >1,000-fold, which makes this step the rate-limiting step for the actin-activated ATP hydrolysis cycle of M5aFull. The ADP off rate from acto-M5aFull was decreased by ~10-fold, and the equilibrium between the prehydrolysis state and the post hydrolysis state was shifted toward the former state in the inhibited state of M5aFull. Because of these changes, M5aFull spends a majority of the ATP hydrolysis cycling time in the weak actin binding state. The present results indicate that M5aFull molecules at a low [Ca^{2+}] is inhibited as a cargo transporter not only due to the decrease in the cross-bridge cycling rate but also due to the decrease in the duty ratio thus being dissociated from actin.

During a past decade, a number of myosin-like proteins have been found, and they are often called unconventional myosin because they fail to form thick filaments, one of the characteristics of "myosin" (for reviews, see Refs. 1 and 2). Among them, class V myosin is best studied, because its function seems to be quite different from conventional myosin. The most intriguing finding is that myosin Va can travel for a long distance without dissociating from actin filaments (for a review, see Ref. 3) unlike conventional myosin. This feature has been termed "processive," and it is thought that myosin Va functions as a cargo transporter rather than a force producer in cells (4–8). Evidence has accumulated that myosin V is involved in vesicular transport in a variety of cell types (for a review, see Ref. 9). Myosin Va transports melanosomes in melanocytes in vertebrates (10–13). It is also shown that endosomal vesicles are transported by myosin Vb and Vc in cultured cells (14, 15). However, these vesicles are not always moved around and the transport process must be regulated by all means. One way to explain such a regulation of myosin V-based vesicle transport is the binding of myosin V to cargos. It was reported that the phosphorylation of myosin V down-regulates the vesicle transport in mitotic cells due to the dissociation from the vesicles (12). The other is the direct regulation of the motor activity of myosin V. Recent biochemical studies have indicated that the regulation of the motor activity involves the interdomain interaction of myosin V (16, 17). Myosin Va is a two-headed myosin with two identically conserved head motor domains and the light chain binding domain consisting of six IQ sequences, IQ*XXX*RG*XXX*R, as light chain binding sites. The dimer formation is achieved with a coiled-coil structure downstream of the IQ domain. This is followed by a series of flexible linkers and the predicted coiled-coil sequences. The C-terminal ~400 amino acids of myosin Va form a globular tail domain mediating myosin Va recruitment to specific organelles, such as melanosome (10, 18–20).

The actin-activated ATPase activity of full-length myosin Va (M5aFull)[2] is significantly inhibited at low Ca^{2+}, whereas those of heavy meromyosin (HMM) or subfragment 1 (S1)-like constructs are not inhibited and constitutively active (16, 17), suggesting that the C-terminal globular tail plays an important role in the Ca^{2+}-dependent regulation. By sedimentation analysis and electron microscopic observation, it was shown that myosin Va forms a folded conformation at low Ca^{2+} in which the tail domain is folded back toward the head, whereas it forms an extended conformation in high Ca^{2+} (16, 17, 21). Of interest is that the conformational transition is closely correlated with activation of the actin-activated ATPase activity of myosin Va (16, 17, 21). Because the lack of the tail domain abolishes the regulation, a model has been proposed, in which the tail domain interacts with and inhibits the myosin Va motor activity, and high Ca^{2+} abolishes the interaction between the head and tail domains, thus activating the actin-activated ATPase activity, presumably due to the conformational change of calmodulin (CaM) light chain.

[2] The abbreviations used are: M5aFull, full-length myosin Va; HMM, heavy meromyosin; S1, subfragment 1; CaM, calmodulin; Mant, methyl-anthraniloyl-; mdATP, 3'-Mant-2'-deoxy-ATP; mdADP, 3'-Mant-2'-deoxy-ADP; PBP, phosphate-binding protein; MDCC, 7-diethylamino-3-((((2-maleimidyl)ethyl)amino)carbonyl)-coumarin; M, myosin Va; AM, actomyosin Va; MOPS, 4-morpholinepropanesulfonic acid.

As described above, one of the most important motor properties of myosin V is its processivity, and this is closely correlated with the high duty ratio of myosin V. Because the high duty ratio myosin spends the majority of the cross-bridge cycle in the strong actin-binding form, it can move processively on actin filaments with possible cooperativity between the two heads. A critical question is whether the inhibition of the ATPase cycle at low Ca^{2+} is simply due to the decrease in the overall cycling rate or involves the change in the hydrolysis cycle mechanism that possibly affects the processive nature of myosin V. In this study, we analyzed the effect of Ca^{2+} on the kinetic mechanism of actin-activated ATPase reaction of the full-length myosin Va to address this question. Our results suggest that the decrease in the Ca^{2+} not only reduces the overall cycling rate but also changes the duty ratio of myosin Va.

EXPERIMENTAL PROCEDURES

Materials—*Escherichia coli* strains XL1-Blue and DH10BAC were purchased from Stratagene (San Diego, CA), and Invitrogen, respectively. Restriction enzymes and modifying enzymes were purchased from New England Biolabs (Beverly, MA). Anti-FLAG M2-agarose, purine nucleotide phosphorylase, 7-methylguanosine, phosphoenolpyruvate, pyruvate kinase, and ADP were from Sigma. Ultrapure grade of ATP was purchased from AMRESCO Inc. (Solon, OH). 3′-Mant-2′-deoxy-ATP (mdATP) and 3′-Mant-2′-deoxy-ADP (mdADP) were kindly provided by Dr. Howard D. White (Eastern Virginia Medical School, Norfolk, VA). Actin was prepared from rabbit skeletal muscle according to Spudich and Watt (22) and used after treatment of phalloidin (Invitrogen). Pyrene-actin was prepared as reported (23, 24). Phosphate-binding protein (PBP) labeled with 7-diethylamino-3-((((2-maleimidyl)ethyl)amino)carbonyl)-coumarin (MDCC) was prepared as previously described (25, 26). Smooth muscle myosin was prepared from turkey gizzard as described (27).

Full-length murine melanocyte-type myosin Va was expressed in Sf9 cells by co-infection of myosin Va heavy chain with CaM viruses and prepared using anti-FLAG antibody affinity column chromatography as described (28). The M5aFull fractions eluted from the affinity column were pooled, concentrated, and dialyzed against buffer A (30 mM KCl, 20 mM MOPS-KOH (pH 7.5), 5 mM 2-mercaptoethanol) containing 2 mM $MgCl_2$ and 0.1 mM EGTA. Typically, 1 mg of protein was obtained from about 5×10^9 cells. The purified M5aFull was stored on ice and used within 3 days. For some experiments, nucleotide-free M5aFull was alternatively prepared by incubating with 0.2 units/ml apyrase at 25 °C for 30 min. The concentration of active sites of M5aFull was determined by using [2,8-^{3}H]ADP/VO_4. The unbound [2,8-^{3}H]ADP/VO_4 was removed using a 0.45-μm nitrocellulose filter, and the bound [2,8-^{3}H]ADP/VO_4 was detected by liquid scintillation counting.

Steady-state ATPase Assay—The assay of steady-state ATPase activity was carried out at 25 °C in the presence of an ATP regeneration system. The assay was done in buffer A containing 3 mM $MgCl_2$, 2 mM ATP, 5 μM CaM, 20 units/ml pyruvate kinase, 2.5 mM phosphoenolpyruvate, 1 mM EGTA or 0.2 mM $CaCl_2$, 10–100 μg/ml M5aFull, and various concentrations of F-actin from 0 to ~20 μM. The liberated pyruvate was determined as described previously (29).

Kinetic Measurements—The quenched flow measurements were performed at 25 °C using a Kin-Tek RQF-3 apparatus (Kin-Tek Corp., Clarence, PA) in buffer A plus 2 mM $MgCl_2$, 5 μM CaM, 1 mM EGTA or 0.2 mM $CaCl_2$, and [γ-^{32}P]ATP. M5aFull (1.85 μM head) and 0.4 μM [γ-^{32}P]ATP were mixed, held in a delay line at the various times, and quenched by a second mix with 0.2 M perchloric acid and 50 mM NaH_2PO_4. The solution was then mixed with 1 ml of charcoal slurry, vortexed, and centrifuged to remove the unhydrolyzed ATP (27). The data were fit to a double exponential equation and analyzed as described (25).

Stopped flow measurements were done at 25 °C with a Kin-Tek SF-2001 in buffer A containing 2 mM $MgCl_2$, 5 μM CaM, 1 mM EGTA or 0.2 mM $CaCl_2$. The Mant nucleotides (λ_{ex} = 356 nm) were excited by utilizing the fluorescence resonance energy transfer of tryptophan fluorescence (λ_{ex} = 280 nm), and the fluorescence intensity was monitored using a 420-nm long pass filter. The wavelengths of the excitation and the emission in other experiments were as follows: λ_{ex} = 365 nm with 370 ± 30-nm band pass filter and λ_{em} > 400 nm for pyrene-actin; λ_{ex} = 295 nm and λ_{em} > 340 nm for tryptophan fluorescence; and λ_{ex} = 433 nm with 436 ± 10-nm band pass filter and λ_{em} > 455 nm for MDCC-PBP, respectively. To measure the phosphate release step, 3 μM MDCC-PBP, 0.3 mM 7-methylguanosine, and 0.01 units/ml purine nucleotide phosphorylase were preincubated in all solution before the measurements, and 20 units/ml hexokinase and 2 mM glucose were added in a syringe containing actin to remove the contaminated ATP. The ratio of mixing two solutions was 1:1 in all experiments.

Gel Electrophoresis—SDS-PAGE was carried out on a 4.5–20% polyacrylamide gradient gel according to the method of Laemmli (30). Molecular mass markers used were smooth muscle myosin heavy chain (204 kDa), β-galactosidase (116 kDa), phosphorylase *b* (97.4 kDa), bovine serum albumin (66 kDa), ovalbumin (45 kDa), carbonic anhydrase (29 kDa), myosin regulatory light chain (20 kDa), and α-lactalbumin (14.2 kDa).

Other Measurements—The concentrations of the following reagents and proteins were determined by absorbance using the extinction coefficients reported: ATP and ADP, ϵ_{259} = 15,400; Mant nucleotides, ϵ_{255} = 23,300 (31); actin, ϵ_{290} = 26,600 (32); pyrene-actin, ϵ_{290} = 29,400 (24). Computer simulation was carried out using STELLA software version 8.1.5 (Isee Systems).

RESULTS

Steady-state Actin-activated ATPase Activity of Full-length Myosin Va—Expression and purification of M5aFull (Fig. 1*A*) was done as described previously using anti-FLAG-agarose affinity chromatography (28). The purified M5aFull sample contained 190-kDa heavy chain and CaM light chain, and no significant contaminants were observed (Fig. 1*B*). All the experiments in the present study were done using this preparation. The basal ATPase activity (0.02 s^{-1}) was increased in the presence of actin; however, the actin-activated ATPase activity was significantly influenced by Ca^{2+}, consistent with the previous reports (16, 17) (Fig. 2). The steady-state ATPase activity was measured as a function of actin con-

A

Full length Mouse Myosin Va

B
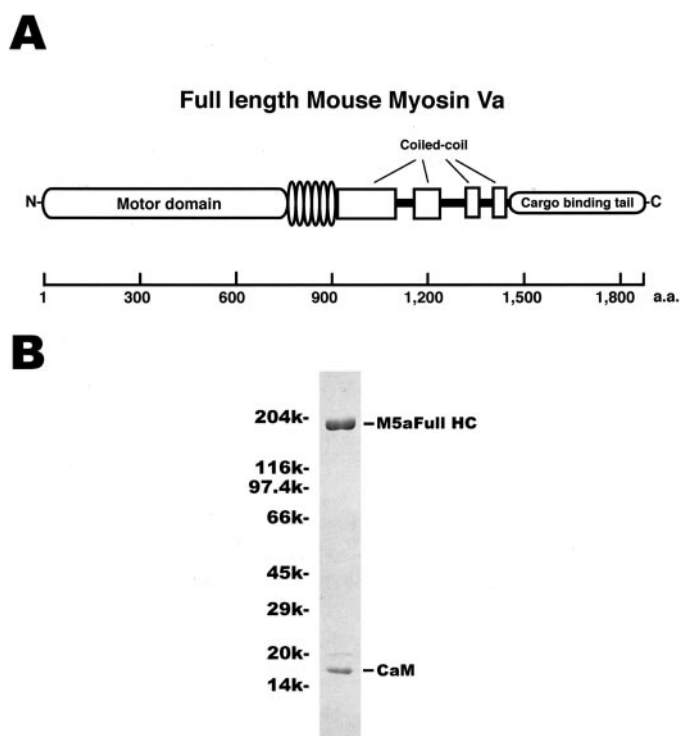
FIGURE 1. **Expression of the full-length mouse myosin Va.** *A*, schematic representation of M5aFull. M5aFull consists of the motor domain, the six IQ motifs, the coiled-coil domains, and the cargo-binding tail domain. CaM can bind to the IQ motifs as the light chains. The coiled-coil domains shown are predicted by using paircoil (available on the World Wide Web at paircoil.lcs.mit.edu/cgi-bin/paircoil (53)). *B*, SDS-PAGE of the purified M5aFull. The M5aFull heavy chain and CaM viruses were co-expressed in Sf9 cells, and the proteins were extracted and purified as described under "Experimental Procedures." The purified proteins were then analyzed by SDS-PAGE. M5aFull HC and CaM represent the heavy chain of M5aFull and CaM, respectively. Molecular masses are shown to the *left*.

centration, and the results were explained with Michaelis-Menten kinetics for both in the presence of 1 mM EGTA and 0.2 mM Ca^{2+}. The obtained V_{max} in the presence of Ca^{2+} was 8-fold larger than that in the presence of EGTA, and the K_{ATPase} value was 5-fold lower in the presence of Ca^{2+} than in its absence. On the other hand, we found that the basal ATPase activity was also influenced by Ca^{2+} (Fig. 2*B*). It has been suggested that the low ATPase activity in the presence of EGTA is due to the formation of the inhibited conformation of myosin Va (16, 17, 21). However, the steady-state ATPase activity in the presence of EGTA may not accurately represent the activity of the inhibited form, because a relatively small fraction of the unregulated myosin Va in the preparation would significantly increase the overall activity of the sample. To accurately determine the ATPase activity in the inhibited and the activated forms, respectively, we performed single turnover experiments. M5aFull was mixed with mdATP and held for 5 s to produce myosin Va (M)·mdADP·P_i intermediate, and then 60 μM actin and the excess amount of nonfluorescent ATP were added and followed the decrease in the fluorescence intensity of the Mant group. After release of the products, the myosin active site binds ATP, but this does not reflect any fluorescence change because of the presence of excess nonfluorescent ATP. The decrease in the fluorescence intensity in Ca^{2+} up to 1 s was fit with a double exponential kinetics, and the observed rate con-
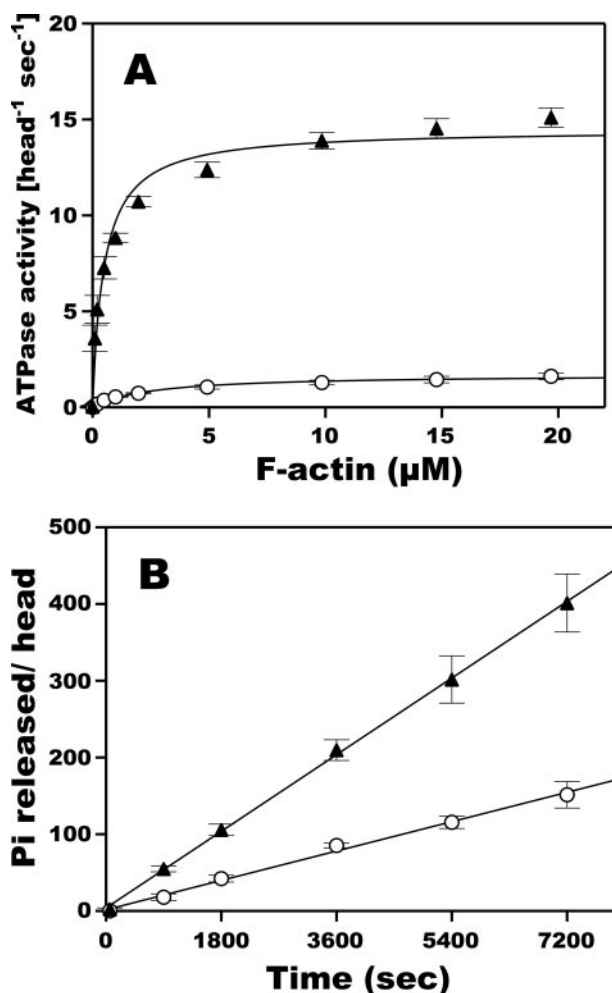
FIGURE 2. **Ca^{2+}-dependent regulation of the steady-state actin-activated ATPase activity of M5aFull.** *A*, actin dependence of the steady-state ATPase activity in the presence of 1 mM EGTA (*open circles*) or 0.2 mM $CaCl_2$ (*closed triangles*). The ATPase activity was measured as described under "Experimental Procedures." *Solid lines* show the best fits to the Michaelis-Menten equation ($V - V_0 = V_{max}$[actin]/K_{ATPase} + [actin]), where V_0 represents the ATPase activity in the absence of actin. The $V_0 + V_{max}$ and K_{ATPase} values are 1.69 $\pm$ 0.09 s^{-1} and 2.6 $\pm$ 0.5 μM in EGTA and 14.4 $\pm$ 0.3 s^{-1} and 0.49 $\pm$ 0.06 μM in Ca^{2+}, respectively. *Error bars*, S.E. from three independent preparations. *B*, the basal ATPase activity of M5aFull. The ATPase activities of M5aFull in EGTA (*open circles*) or Ca^{2+} (*closed triangles*) were measured in the absence of actin and plotted against time. The basal ATPase activities are 0.021 $\pm$ 0.001 s^{-1} in EGTA and 0.055 $\pm$ 0.003 s^{-1} in Ca^{2+} conditions. *Error bars*, S.E. ($n = 4$).

stants (k_{obs}) were 22 $\pm$ 4 and 3.5 $\pm$ 1.9 s^{-1} for the fast and slow rates, respectively (Fig. 3*B*). On the other hand, the rate constant of the major fraction (~65% in amplitude) observed in the presence of EGTA was 0.06 $\pm$ 0.01 s^{-1} with the minor phase of faster rate (0.31 $\pm$ 0.05 s^{-1}, ~20% in amplitude) (Fig. 3*A*). We could also observe the rapid phase (28 $\pm$ 4 s^{-1}), similar to the rate obtained in Ca^{2+}. The fraction of the initial rapid phase in EGTA was approximately ~15%, and this is thought to be due to the presence of the unregulated molecules. We expect that the rate constants obtained in this actin concentration are nearly saturated and thus similar to the V_{max} values; nevertheless, the activity in EGTA was ~30-fold lower than that obtained from the steady-state rate (Fig. 2). The result suggests that there is ~15% of unregulated myosin Va present in the preparation. Fig. 3*C* shows the ATP single turnover rates of
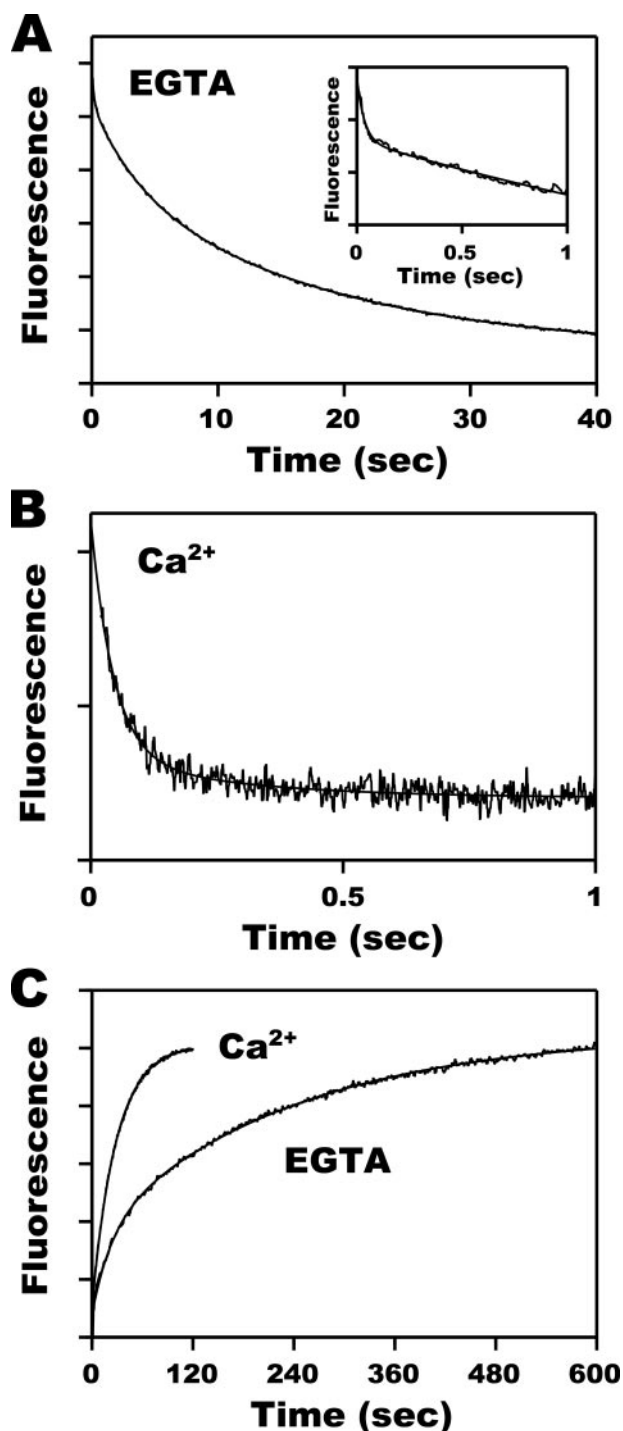
FIGURE 3. **Single turnover experiments of the actin-activated ATPase activity of M5aFull.** *A* and *B,* single turnover rates in the presence of actin. The experiments were done in the presence of 1 mM EGTA (*A*) or 0.2 mM CaCl₂ (*B*). At 5 s after mixing M5aFull (0.3 μM head) with 3 μM mdATP, the solution was mixed with 60 μM F-actin plus 3 mM MgATP (before mix). The *panels* shown are the average of three fluorescence results. The observed rate constants (k_{obs}) were obtained by fitting the time course to a double ($I(t) = I_{fast}e^{-k_{obs}1t} + I_{slow}e^{-k_{obs}2t} + C$) or triple ($I(t) = I_{fast}e^{-k_{obs}1t} + I_{middle}e^{-k_{obs}2t} + I_{slow}e^{-k_{obs}3t} + C$) exponential equations. The *inset* in *A* shows a rapid decrease in fluorescence intensity within 1 s. The fast, middle, and slow k_{obs} values in the presence of EGTA are 28 ± 4 s⁻¹ (~15% of total amplitude), 0.31 ± 0.05 s⁻¹ (~20%), and 0.06 ± 0.01 s⁻¹ (~65%), respectively. The fast and slow k_{obs} values in the presence of Ca²⁺ are 22 ± 4 s⁻¹ (~75% of total amplitude) and 3.5 ± 1.9 s⁻¹ (~25%), respectively. The *error bars* indicate the S.E. (*n* = 3). *C,* single turnover rates in the absence of actin. The experiments were performed in the presence of 1 mM EGTA or 0.2 mM CaCl₂. At 5 s after

M5aFull without actin in the presence of EGTA and Ca²⁺. In this experiment, M5aFull was first mixed with unlabeled ATP and held for 5 s, and then an excess amount of Mant-ATP was added. Although the increase in the fluorescence intensity in EGTA followed a double exponential kinetics, the change in the intensity in Ca²⁺ followed a single exponential kinetics. The k_{obs} values were 0.02–0.03 s⁻¹ (~30% in amplitude) and 0.003–0.004 s⁻¹ (~70% in amplitude) for fast and slow rates in the presence of EGTA, respectively, and 0.03–004 s⁻¹ in the presence of Ca²⁺. This result also indicates that Ca²⁺ regulation is effective even in the absence of actin, and ATPase activity in the EGTA condition is inhibited.

ATP Binding to Full-length Myosin Va—The rate of ATP binding to M5aFull was determined by measuring the change in the fluorescence intensity of mdATP upon binding (not shown). The experiments were done in the absence and presence of actin. The time courses of fluorescence enhancement were fit by single exponential kinetics for both in EGTA and Ca²⁺. The k_{obs} values showed a linear dependence on the mdATP concentration to yield the apparent second order rate constants ($K_1k_{+2\,(app)}$) of 1.91 ± 0.04 μM⁻¹ s⁻¹ and 1.80 ± 0.03 μM⁻¹ s⁻¹ in the EGTA and Ca²⁺, respectively. In the presence of actin, the apparent second order rate constants ($K_1'k_{+2(app)}'$) were 1.38 ± 0.02 and 3.1 ± 0.3 μM⁻¹ s⁻¹ in EGTA and Ca²⁺, respectively. The obtained values were similar to that previously reported for the S1 construct (33–35). It should be noted that the treatment of the samples with apyrase that eliminates any contaminated ADP did not alter the rate of ATP binding. This indicates that there was no contamination of ADP in the samples.

ATP-induced Production of the Weak Actin Binding State of Actomyosin Va—The kinetics of ATP-induced transition of M5aFull from the rigor state to the weak actin binding state was monitored by measuring the changes in fluorescence intensity of pyrene-labeled actin (Fig. 4). The increase in the pyrene fluorescence upon the formation of "weak" actin-binding form of M5aFull was analyzed by a single exponential kinetics, and the k_{obs} showed hyperbolic saturation curves on the ATP concentration (Fig. 4). The initial slope (Fig. 4, *inset*) of the curve represents a second order rate constant of ATP binding to acto-M5aFull ($K_1'k_{+2}'$). The $K_1'k_{+2}'$ values obtained from the change in pyrene fluorescence were 1.6 ± 0.4 and 3.4 ± 0.4 μM⁻¹ s⁻¹ in EGTA and Ca²⁺, respectively. These values are similar to those obtained from mdATP binding, suggesting that the Mant-moiety does not significantly influence the ATP binding rate to M5aFull. The maximal rates for the transition to the weak actin binding state were estimated from the hyperbolic curves to be 664 ± 66 s⁻¹ and 694 ± 60 s⁻¹, respectively, in EGTA and Ca²⁺.

ATP-induced Enhancement of Intrinsic Tryptophan Fluorescence—It is known that the intrinsic tryptophan fluorescence intensity increases upon the addition of ATP, and this reflects the change in the conformation of myosin motor

mixing 0.15 μM M5aFull (0.3 μM head) with 3 μM ATP, the solution was mixed with 0.1 mM Mant-ATP (before mix). The fast rate, 0.02 s⁻¹ (~30% of total amplitude), and slow rate, 0.003 s⁻¹ (~70%), were observed in EGTA, and a single rate constant (0.04 s⁻¹) was seen in Ca²⁺.
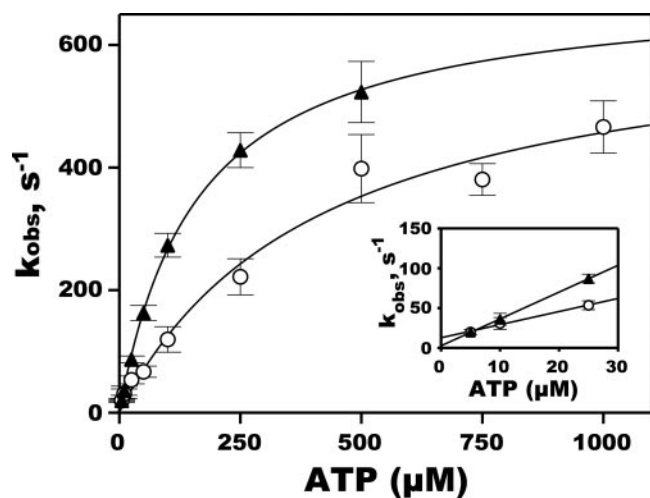
FIGURE 4. **ATP-induced production of the weak actin binding state.** The rates of transition of acto-M5aFull to the weak actin binding state were determined in the presence of 1 mM EGTA (*open circles*) or 0.2 mM CaCl$_2$ (*closed triangles*) by measuring pyrene-actin fluorescence intensity. Acto-M5aFull (0.5 μM myosin head + 0.6 μM pyrene-actin) was mixed with MgATP to give the indicated concentrations of ATP. The time course of change in the fluorescence signal was then monitored. The k_{obs} values were obtained by fitting the fluorescence data to a single exponential equation, ($I(t) = I_0 e^{-k_{obs}t} + C$). *Solid lines* through the data are fit to a hyperbolic equation, $k_{obs} = k_{max}/(1 + K_{app}/[MgATP])$. The fit values for the EGTA condition (*open circles*) were as follows: $k_{max} = 664 \pm 66$ s^{-1} and $K_{app} = 424 \pm 97$ μM. The fit values for the Ca^{2+} condition (*closed triangles*) were as follows: $k_{max} = 694 \pm 60$ s^{-1} and $K_{app} = 161 \pm 37$ μM. The *inset* represents the initial slope in low concentrations of MgATP. The observed second order rate constants are 1.6 ± 0.4 μM^{-1} s^{-1} in EGTA and 3.4 ± 0.4 μM^{-1} s^{-1} in Ca^{2+} conditions. The *error bars* show the S.E. (*n* = 3–10).

FIGURE 5. **ATP-induced enhancement of intrinsic tryptophan fluorescence intensity of M5aFull.** M5aFull (1 μM head) in the presence of 1 mM EGTA (*open circles*) or 0.2 mM CaCl$_2$ (*closed triangles*) was mixed with MgATP to obtain the indicated concentrations of ATP, and the time course of the tryptophan fluorescence change was monitored. The fluorescence data were fitted to the single exponential equation shown in Fig. 4. The k_{obs} values from the data are plotted against ATP concentration. The *solid lines* show the best fits to the hyperbolic equation described in Fig. 4. The k_{max} and K_{app} are 331 ± 35 s^{-1} and 185 ± 48 μM in EGTA and 240 ± 33 s^{-1} and 216 ± 70 μM in Ca^{2+} conditions, respectively. The *inset* shows the representative traces at 2.5 μM MgATP (in final) in EGTA (*lower trace*) and Ca^{2+} (*upper trace*) conditions. *Error bars*, S.E. (*n* = 3–7).

domain (*i.e.* the formation of the M·ADP·P$_i$ ternary complex) (36, 37). M5aFull increased the tryptophan fluorescence intensity after the addition of ATP with single exponential kinetics (Fig. 5, *inset*). The ATP dependence of the k_{obs} showed a hyperbolic saturation curve to yield the maximum rate constants of 331 ± 35 and 240 ± 33 s^{-1} in EGTA and Ca^{2+}, respectively (Fig. 5). The obtained values are also consistent with those previously reported for the S1 constructs of myosin Va (33, 35). The maximum value was significantly lower than k'_{+2}, suggesting that the value represents $k_{+3} + k_{-3}$. It should be noted that the amplitude of the increase in the fluorescence intensity was significantly lower in the presence of EGTA. This result suggests that Ca^{2+} influences the fraction of the intermediate showing enhanced tryptophan fluorescence intensity.

Effect of Ca^{2+} on P$_i$ Burst of Full-length Myosin Va—It is known that the initial rapid P$_i$ release is observed for myosin ATPase reaction when the reaction is quenched by acid, called initial P$_i$ burst. This is due to the formation of M·ADP·P$_i$ ternary complex after ATP hydrolysis. Using a quenched flow apparatus, we measured the rapid initial ATP hydrolysis kinetics. We performed single turnover experiments in which the active site concentration was in excess of the given ATP concentration. In this condition, all of the added ATP bound to the active site even if the measured protein concentration was a little overestimated; therefore, we can accurately determine the amplitude of the P$_i$ burst. Furthermore, the active site concentration of the samples was accurately determined by ADP/vanadate trap experiments (see "Experimental Procedures"). Although the maximum rate constant of the hydrolysis step cannot be obtained with this condition, the equilibrium constant of the

hydrolysis step (K_3) is more accurately estimated than the multiturnover condition. 0.4 μM [γ-^{32}P]ATP was mixed with M5aFull (1.85 μM head), and the time course of P$_i$ release was monitored (Fig. 6). P$_i$ was rapidly released from acto-M5aFull, followed by slow steady-state P$_i$ release. The rates of initial rapid ATP hydrolysis were 0.4 and 0.5 s^{-1}, respectively, in the presence of EGTA and Ca^{2+}, which are consistent with the ATP binding rates of the given conditions. The slow phase in Ca^{2+} was consistent with the steady-state rate and the single turnover experiment of the basal ATPase reaction (Figs. 2*B* and 3*C*). The slow phase in EGTA (0.003 s^{-1}) was also consistent with the predominant phase of the single turnover rate in the absence of actin (0.003–0.004 s^{-1}) (Fig. 3*C*). We think that the relatively high basal ATPase activity in EGTA is due to the presence of unregulated population in the sample. If the activity of unregulated fraction is the same as that of Ca^{2+} condition, the fraction of unregulated M5aFull would be 15–20%. This is consistent with that estimated from the difference in the actin-activated ATPase activities estimated from the single turnover experiment and the steady-state rate. The most intriguing finding is that the P$_i$ burst size was significantly different between the Ca^{2+} and EGTA conditions. From the ratio of the fraction of the fast phase to the slow phase, the P$_i$ burst sizes of 0.20 ± 0.02 mol/mol and 0.78 ± 0.04 mol/mol were obtained, respectively, in the presence of EGTA and Ca^{2+}. Although the P$_i$ burst size in Ca^{2+} was consistent with unregulated myosin Va S1 (33, 38), the P$_i$ burst size in EGTA was much smaller than that in Ca^{2+}. The low P$_i$ burst size in EGTA indicates that a significant population of the full-length myosin Va is present at a prehydrolysis step (M·ATP). The result indicates that the equilibrium of M·ATP-M·ADP·P$_i$ step is significantly shifted to the prehydrolyzed form in the EGTA condition.
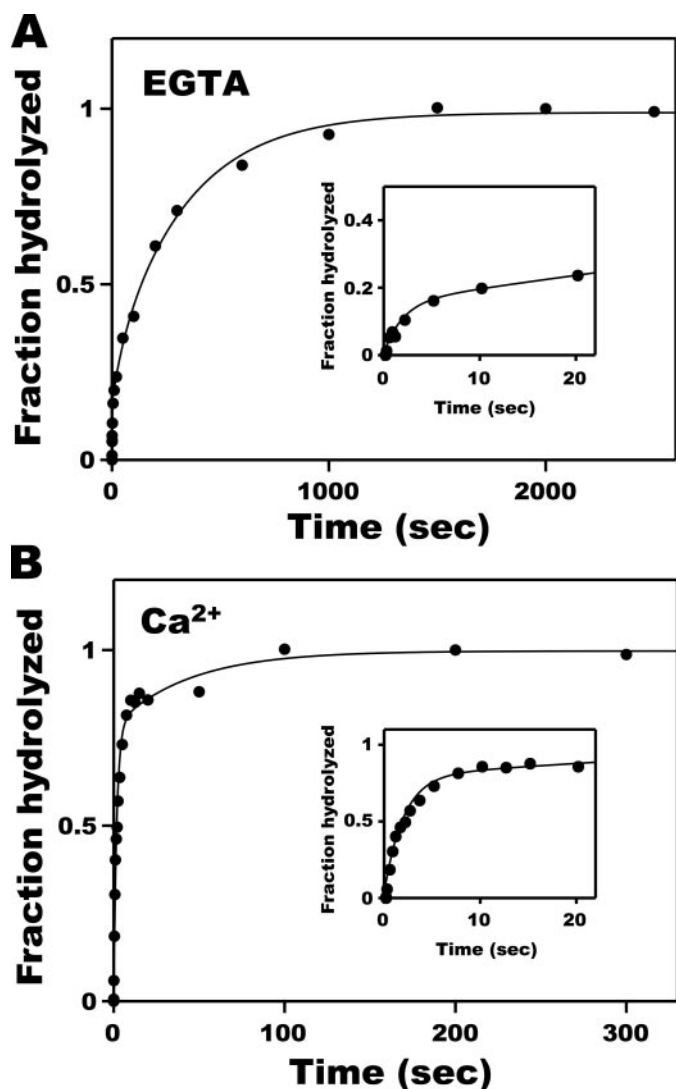
FIGURE 6. **Effect of Ca²⁺ on P_i burst of M5aFull.** M5aFull (1.85 μM head) in the presence of 1 mM EGTA (*A*) or 0.2 mM CaCl₂ (*B*) was mixed with 0.40 μM Mg[γ-³²P]ATP and quenched with acid at various time points. The released P_i was then measured as described under "Experimental Procedures." The fractions of hydrolyzed ATP are plotted against time. The *solid lines* are fit to a double exponential equation, ($l(t) = l_{fast} e^{-k_{obs1}t} + l_{slow} e^{-k_{obs2}t}$). The fit values of fractional amplitudes of the initial P_i burst phase ($l_{fast}/(l_{fast} + l_{slow})$) in EGTA and Ca²⁺ conditions are 0.2 and 0.78, respectively. The fit values of the k_{obs1} and k_{obs2} are 0.4 s⁻¹ and 0.003 s⁻¹ in EGTA and 0.5 s⁻¹ and 0.04 s⁻¹ in Ca²⁺ conditions, respectively. The *insets* show the early phase of the time course.

Rate of P_i Release from Full-length Myosin Va—The rate of P_i release from acto-M5aFull was determined by measuring the increase in fluorescence intensity of MDCC-PBP as described previously (25, 26, 39). M5aFull and ATP were first mixed, held for 5 s to allow ATP binding and hydrolysis, and then mixed with actin. As shown in Fig. 7*A*, the rate constant of the predominant phase in EGTA in the presence of actin was not much larger than that in the absence of actin. The observed rate constant increased hyperbolically with actin concentration for both high and low Ca²⁺ conditions.

In the presence of EGTA, the rate of the predominant phase (∼70%) was slow with the maximum rate of 0.037 ± 0.002 s⁻¹ (Fig. 7*B*). We observed a minor fast phase (∼20% in amplitude) that also increased with actin concentration to reach the maximum rate of 97 ± 9 s⁻¹, which is likely to be due to the pres-
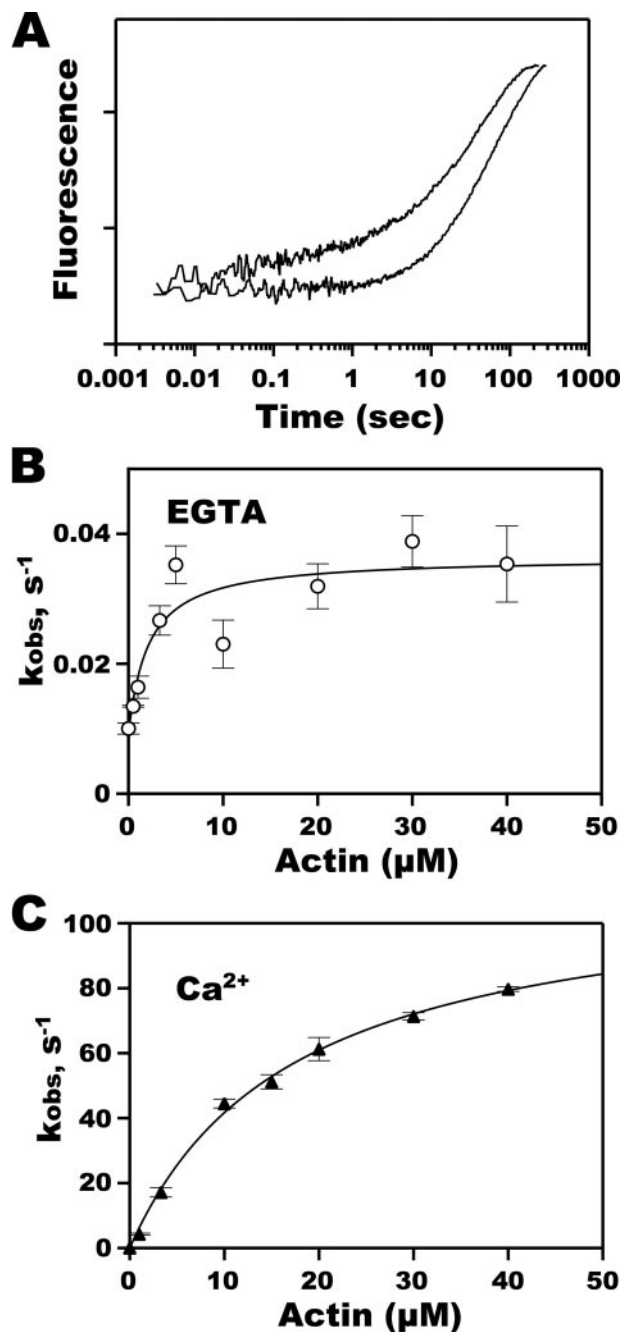
FIGURE 7. **Rate of P_i release from M5aFull.** *A*, time courses of the fluorescence change of MDCC-PBP in the EGTA condition. The data shown are the experiments in the presence of 20 μM (in final, *left*) and absence (*right*) of F-actin. At 5 s after mixing M5aFull (1 μM head) with 0.7 μM ATP, the solution was sequentially mixed with F-actin, and the change in the fluorescence intensity was monitored. *B* and *C*, predominant rates of P_i release from M5aFull in the presence of 1 mM EGTA (*B*) or 0.2 mM CaCl₂ (*C*). Time courses of the change in the fluorescence intensity of MDCC-PBP were monitored in the presence of the indicated concentrations of F-actin (in final). The obtained fluorescence data were fitted to the double or triple exponential equations shown in Fig. 3. The predominant rate constants were the slowest one (∼70% in total amplitude) in EGTA and the fastest one (∼70%) in Ca²⁺. The k_{obs} values are plotted as a function of F-actin concentration. The *solid lines* are the best fits to a hyperbolic equation, $k_{obs} = k_{max}/(1 + K_{app}/[actin])$. The fit values of k_{max} and K_{app} were 0.037 ± 0.002 s⁻¹ and 2 ± 1 μM in EGTA and 113 ± 7 s⁻¹ and 17 ± 2 μM in Ca²⁺ conditions, respectively. The observed second order rate constants are 0.0048 ± 0.0008 μM⁻¹ s⁻¹ in EGTA and 4.4 ± 0.1 μM⁻¹ s⁻¹ in Ca²⁺ conditions. *Error bars*, S.E. (n = 3–10).

ence of unregulated molecules. On the other hand, the predominant phase (~70%) of the P_i release rates in the presence of Ca^{2+} was 113 ± 7 s^{-1} (Fig. 7C). This value was quite similar to the P_i release rate (k'_{+4}) determined with the S1 construct of myosin Va (40). The slow rate (~30%) showed little actin dependence, with rates of ~1 s^{-1}, >100-fold slower than the maximum rate of the fast phase. This slow rate is probably due to the ATP rebinding as shown by Homma and Ikebe (39), because the addition of hexokinase/glucose (ATP removal) greatly diminished the amplitude. A similar rate of a minor phase (~10%) was also observed in the EGTA condition. According to the tangent of the actin dependence of k_{obs}, the second order rate constants ($k'_{+4}/K_{9\,obs}$) of 0.0048 ± 0.0008 and 4.4 ± 0.1 $\mu M^{-1}\,s^{-1}$ were obtained in the presence of EGTA and Ca^{2+}, respectively. These results suggest that the rate of P_i release limits the entire ATP hydrolysis cycle in the inhibited state of M5aFull, because the major fraction of the observed rate (0.04 s^{-1}) was similar to the major fraction of the single turnover rate (0.06 s^{-1}). On the other hand, this step is not the rate-limiting in the active state of M5aFull, because the rate, 113 s^{-1}, was 5 times higher than the single turnover rate (22 s^{-1}).

The Interaction of ADP with Actomyosin Va—The rate of ADP binding to acto-M5aFull was determined by measuring the fluorescence change of Mant-ADP upon binding. The increase in the fluorescence intensity followed double exponential kinetics for both in EGTA and Ca^{2+}, and the apparent rate constants increased with the mdADP concentration. The fast (70–80% of the amplitude) and slow second order rate constants obtained were 7.5 ± 0.2 and 0.48 ± 0.07 $\mu M^{-1}\,s^{-1}$ in the presence of EGTA and 8.5 ± 0.6 and 0.8 ± 0.2 $\mu M^{-1}\,s^{-1}$ in the presence of Ca^{2+}, respectively (Fig. 8A). The ADP binding rate was not much influenced by Ca^{2+}. On the other hand, the result suggested that the ADP dissociation rate from actomyosin Va is significantly affected by Ca^{2+}. The dissociation rate constant can be obtained from the y intercept of the mdADP dependence of k_{obs}. As shown in Fig. 8A, the y intercept values for the fast and slow rates in the EGTA were 4 ± 1 s^{-1} and 1.7 ± 0.2 s^{-1}, respectively, whereas those in Ca^{2+} were 18 ± 2 and 4 ± 1 s^{-1}, respectively. To more accurately determine the ADP release rate, M5aFull was mixed with mdADP, and then we monitored the decrease in the fluorescence intensity of Mant group after the addition of excess ATP (Fig. 8, B and C). The decrease in fluorescence intensity in Ca^{2+} was biphasic and followed double exponential kinetics (Fig. 8C). The k_{obs} values were 23.3 ± 0.8 and 3.5 ± 0.2 s^{-1} for the fast and slow phases with the amplitude of ~75 and ~25%, respectively. The weight-averaged rate of mdADP release in the presence of Ca^{2+} (18 s^{-1}) was similar to that of the steady-state ATPase cycle rate, suggesting that the ADP release from actomyosin Va limits the entire ATP hydrolysis cycle rate in Ca^{2+}. The double exponential kinetics for the ADP off step was previously reported for the unregulated HMM construct, which was proposed to be due to the interaction between the two heads (41).

On the other hand, the rate of mdADP release in EGTA was much slower than those obtained in Ca^{2+} (Fig. 8B). The predominant phase (~55%) with a rate constant of 3.0 ± 0.3 s^{-1} was followed by the minor phase (~25%) with a rate constant of
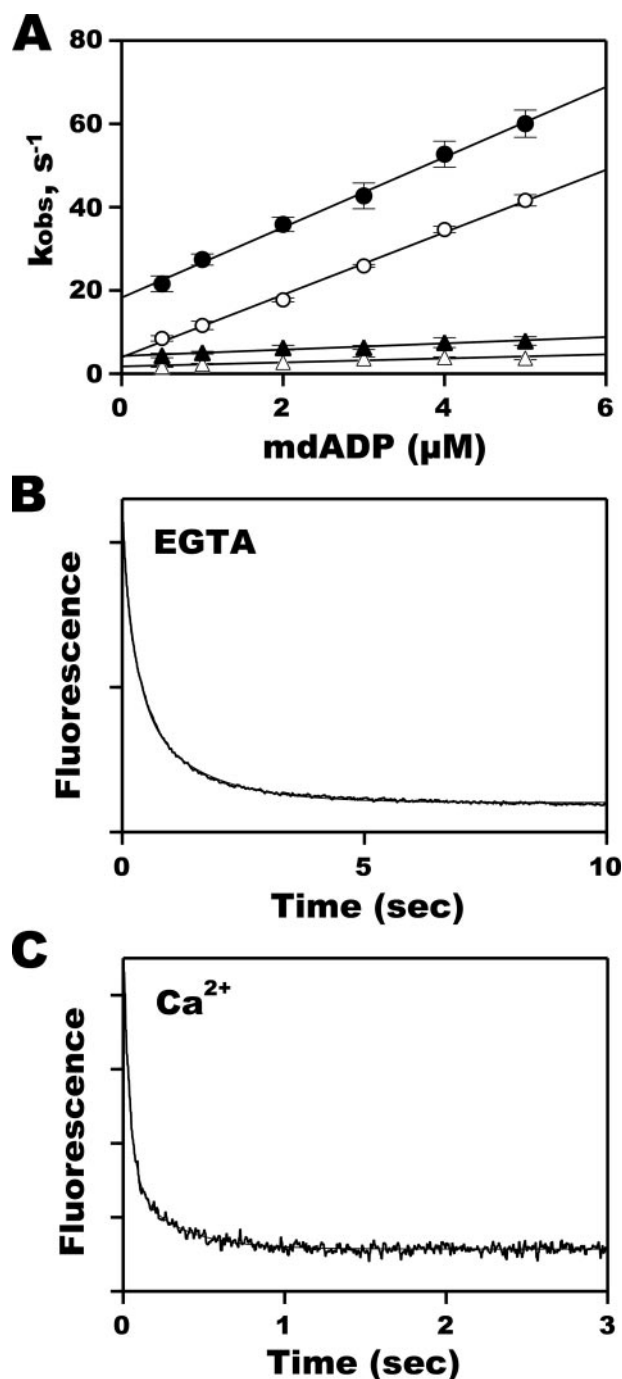
FIGURE 8. **The interaction of Mant-ADP with acto-M5aFull.** *A*, Mant-ADP binding to acto-M5aFull in the presence of 1 mM EGTA (*open symbols*) and 0.2 mM $CaCl_2$ (*closed symbols*). Acto-M5aFull (0.2 μM M5aFull head plus 0.24 μM actin) was mixed with mdADP to give the indicated concentrations of mdADP, and the increase in fluorescence intensity was monitored. The results were fitted to the double exponential equation shown in Fig. 3. The k_{obs} values are plotted as a function of mdADP concentration. The observed second order rate constants (K'_{-5}) for the fast (*circles*) and slow (*triangles*) rates: 7.5 ± 0.2 and 0.48 ± 0.07 μM^{-1} s^{-1} in EGTA and 8.5 ± 0.6 and 0.8 ± 0.2 $\mu M^{-1}\,s^{-1}$ in Ca^{2+} conditions, respectively. *Error bars*, S.E. (n = 3 or 4). *B* and *C*, dissociation of Mant-ADP from acto-M5aFull in the presence of 1 mM EGTA (*B*) and 0.2 mM $CaCl_2$ (*C*). Acto-M5aFull (0.2 μM myosin head) pre-equilibrated with 5 μM mdADP was mixed with 1.5 mM MgATP (before mix), and the increase in the fluorescence intensity was monitored. The obtained fluorescence data were fitted to the double or triple exponential equations described in the legend to Fig. 3. The k_{obs} values (K'_{+5}) are 11 ± 1 s^{-1} (~20% in total amplitude), 3.0 ± 0.3 s^{-1} (~55%), and 0.66 ± 0.06 s^{-1} (~25%) for the fast, middle, and slow rates in EGTA and 23.3 ± 0.8 s^{-1} (~75% in total amplitude) and 3.5 ± 0.2 s^{-1} (~25%) for the fast and slow rates in Ca^{2+}, respectively. *Error bars*, S.E. (n = 4–10).

$0.66 \pm 0.06\,\text{s}^{-1}$ (Fig. 8*B*). These values are consistent with those estimated in Fig. 8*A*. It should be noted that there was a minor initial rapid phase ($\sim$20%) having a similar rate constant to that in Ca^{2+}, and it is likely that this is due to the presence of unregulated molecules in the preparation.

The marked decrease in the ADP release rate from actomyosin Va in EGTA was also shown by measuring the ATP-induced change in the fluorescence of pyrene-actomyosin Va. The rate of the change in the fluorescence of pyrene-actomyosin Va increased with ATP, but unlike the result shown in Fig. 4, the rate was saturated at a lower ATP concentration in the presence of ADP. This is because the actomyosin Va dissociation is limited by the ADP release step.

The saturated k_{obs} values of the ATP dependence of Fig. 9 were 3.7 ± 0.3 and $0.8 \pm 0.1\,\text{s}^{-1}$ with $\sim$45 and $\sim$35% of the total amplitude. The fast rate of $20\text{–}30\,\text{s}^{-1}$ was also observed with an amplitude of less than 20%, which is likely to be due to the unregulated molecules. In the presence of Ca^{2+}, the k_{obs} values for the predominant fast phase ($>$50%) was $26 \pm 2\,\text{s}^{-1}$. The results further support the possibility that the ADP release rate is significantly reduced at low concentration of Ca^{2+}. Although the ADP release rate in the absence of Ca^{2+} is much lower than that in the presence of Ca^{2+}, the rate is significantly higher than the overall cycling rate observed in Fig. 3*A*.

DISCUSSION

Kinetic Mechanism of the Full-length Myosin Va—In the present study, we clarified the mechanism of the inhibition of the ATPase activity of mammalian myosin Va at low Ca^{2+} by kinetic analysis of the actin-activated ATP hydrolysis cycle. Three major effects of lowering Ca^{2+} on the elementary kinetic steps were found. First, the rate of ADP release from actomyosin Va (AM)·ADP complex is significantly decreased by 10-fold at low Ca^{2+} (*i.e.* in EGTA). The rate constant of the ADP release step from AM·ADP in high Ca^{2+} was comparable with the entire ATP hydrolysis cycling rate in this condition, indicating that this step is the rate-determining step of actomyosin Va ATPase cycle in high Ca^{2+}. Although the rate of ADP release was significantly decreased at low Ca^{2+}, the ADP off rate is still faster than the overall cycle rate of actomyosin Va at low Ca^{2+}. The result suggested that the ADP off step is not the rate-determining step for actomyosin Va ATPase reaction at low Ca^{2+} in contrast to that at high Ca^{2+}. Since the ATP binding step and the subsequent ATP hydrolysis step in the presence of physiological ATP concentration are much faster than the ATPase cycle rate at low Ca^{2+}, we thought that the actin rebinding and the following P_i release from AM·ADP·P_i limit the entire cycle rate at low Ca^{2+}. As a result, we found that the rate of P_i release from AM·ADP·P_i complex is decreased more than 1,000-fold by lowering Ca^{2+} concentration. At high Ca^{2+}, the P_i release rate constant from the AM·ADP·P_i complex was at least 5-fold larger than the entire ATP hydrolysis cycle rate, thus not rate-determining. The marked decrease in the P_i off rate from the AM·ADP·P_i complex at low Ca^{2+} makes the rate of this step comparable with the entire ATP hydrolysis cycling rate. The result suggests that the P_i release step becomes the rate-determining step in the inhibited state of the full-length myosin Va.
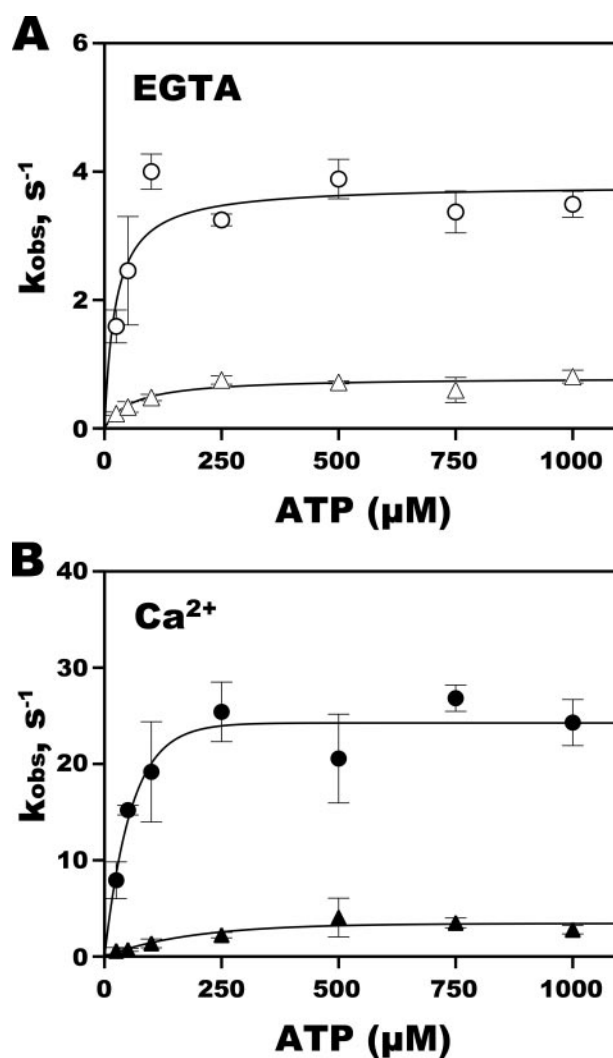
FIGURE 9. **ATP induced dissociation of pyrene-actin from acto-M5aFull·ADP complex.** The rates of ADP dissociation in the presence of 1 mM EGTA (*A*) or 0.2 mM $CaCl_2$ (*B*) were determined by measuring the time course of the change in pyrene-actin fluorescence intensity. Acto-M5aFull (0.5 μM myosin head plus 0.6 μM pyrene-actin) pre-equilibrated with 50 μM MgADP was mixed with MgATP to obtain the indicated concentration of MgATP in the flow cell. The time course of fluorescence enhancement followed triple exponential kinetics. The obtained k_{obs} values are plotted as a function of ATP concentration. *Solid lines* through the data are the best fits to the hyperbolic equation described in Fig. 4. The fit values in EGTA were as follows: for the fast phase ($\sim$20% in total amplitude; not shown), $k_{max} = 27 \pm 3\,\text{s}^{-1}$ and $K_{app} = 229 \pm 87$ μM; for the medium phase ($\sim$45%; *open circles*), $k_{max} = 3.7 \pm 0.3\,\text{s}^{-1}$ and $K_{app} = 23 \pm 10$ μM; for the slow phase ($\sim$35%; *open triangles*), $k_{max} = 0.8 \pm 0.1\,\text{s}^{-1}$ and $K_{app} = 60 \pm 25$ μM. The fit values in Ca^{2+} were as follows: for the fast phase ($\sim$50% in total amplitude, *closed circles*), $k_{max} = 26 \pm 2\,\text{s}^{-1}$ and $K_{app} = 40 \pm 19$ μM; for the medium phase ($\sim$20%, *closed triangles*), $k_{max} = 4.0 \pm 0.8\,\text{s}^{-1}$ and $K_{app} = 168 \pm 108$ μM; for the slow phase ($\sim$30%, not shown), $k_{max} = 0.56 \pm 0.09\,\text{s}^{-1}$ and $K_{app} = 111 \pm 76$ μM. *Error bars*, S.E. ($n = 3\text{–}6$).

Another major effect of Ca^{2+} on the ATP hydrolysis cycle of actomyosin Va is the P_i burst size. Whereas the P_i burst size of the full-length myosin Va at high Ca^{2+} was nearly identical to that previously reported for the unregulated S1 construct (33), the P_i burst size at low Ca^{2+} was 0.2 mol/mol, which is much lower than that at high Ca^{2+}. The P_i burst represents the rapid hydrolysis of ATP by myosin to form M·ADP·P_i ternary complex that is labile by acid quench to release the bound P_i, therefore, the result indicates that a significant fraction of myosin Va is accumulated as the prehydrolysis form during the ATP

hydrolysis cycle at low Ca^{2+}. Because the rate of ATP-induced dissociation of actomyosin Va is fast, it is anticipated that the ATP hydrolysis takes place while myosin Va is dissociated from actin. Therefore, the present result suggests that the low steady-state ATPase rate of actomyosin Va at low Ca^{2+} is due to the combination of the decreased rate of the P_i off and ADP off and the low fraction of $M \cdot ADP \cdot P_i$ ternary complex during the hydrolysis cycle. Among them, the marked decrease in the P_i off rate at low Ca^{2+} is the major component that explains the low ATP hydrolysis cycle in the inhibited state of myosin Va.

We think that the actual P_i burst size in the inhibited state of myosin Va would be much lower than the value determined (~ 0.2), because we estimate the fraction of the active form in the sample to be $0.1–0.2$. If so, the effect of Ca^{2+} on the burst size would be more prominent. A low P_i burst size (~ 0.4) is also reported in unregulated S1 construct having CaM as a light chain, although the size of a construct having LC-1sa was nearly 1.0 (38). Taken together with our findings, the decreased P_i burst size is not due to the conformation specific to the inhibited form with tail but may be due to the conformational change of CaM by Ca^{2+}.

Since a significant fraction of the steady-state intermediate of the full-length myosin Va at low Ca^{2+} is accumulated in $M \cdot ATP$, a weak actin binding intermediate, it is anticipated that the duty ratio of actomyosin Va ATP hydrolysis cycle at low Ca^{2+} is significantly lower than that at high Ca^{2+}. Using the experimentally determined kinetic constants in the present study, the overall ATP hydrolysis cycle pathway of actomyosin Va was analyzed for both high and low Ca^{2+} by using computer simulation. All rate constants and equilibrium constants obtained in the present study are summarized in Table 1. Except for the three steps described above, we found that the kinetic parameters of the actomyosin Va ATPase reaction are not significantly affected by Ca^{2+}. The ATP binding step is fast in the physiological ATP concentration (above 1 mM) and calculated to be >600 s^{-1} (Fig. 4), thus not a rate-determining step. The following dissociation of myosin Va from actin and the ATP hydrolysis steps are also much faster than the overall cycle rate. Although the maximum rate constant for the P_i off step at high Ca^{2+} was not accurately determined, we could estimate that the rate of this step is >100 s^{-1} based upon the result shown in Fig. 7C. Based upon the single turnover experiment, we found that Ca^{2+} activates the ATP hydrolysis cycle rate >100-fold. Although the rate of ADP off step from $AM \cdot ADP$ is decreased by lowering Ca^{2+}, the extremely low ATP hydrolysis cycle rate in low Ca^{2+} can be explained by the inhibited P_i off rate in this condition.

Based on the kinetic parameters determined in the present study, we calculated the steady-state distribution of intermediates during the actomyosin Va ATP hydrolysis cycle under the physiological ATP concentration (~ 4 mM) (Fig. 10A). Both $M \cdot ATP$ ($\sim 23\%$) and $AM \cdot ADP \cdot P_i$ ($\sim 62\%$) are the predominant steady-state intermediates for the actomyosin Va ATP hydrolysis cycle at low Ca^{2+}, whereas only $AM \cdot ADP$ is the predominant intermediate at high Ca^{2+} that explains $\sim 68\%$ of the steady-state intermediates. Basically, the kinetic mechanism of the full-length myosin Va at high Ca^{2+} is almost the same as the one previously reported for unregulated S1 construct (33). On

the other hand, the full-length myosin Va in the inhibited form is present in the weak actin binding states in the presence of ATP. Fig. 10B shows the computer-simulated steady-state ATPase activity of the inhibited form. The V_{max} and K_{ATPase} values calculated by the simulation were 0.033 s^{-1} and 17.7 μM, respectively. This indicates that the maximum ATPase cycle rate of the inhibited state is ~ 500-fold lower than the activated state. The result suggests that myosin Va does not consume ATP in the cells before the activation in which myosin Va begins functioning as a cargo transporter.

While the present study was being conducted, Olivares *et al.* (42) reported the kinetic analysis of the full-length chick myosin Va. They reported that the ADP off rates from equilibrated $AM \cdot Mant$-ADP were biphasic for both in the presence (8.8 and $0.5–1$ s^{-1}) and absence of Ca^{2+} (1.7 and ~ 0.5 s^{-1}). Although the ADP off rate in the presence of Ca^{2+} is slower than that obtained in the present study for mouse myosin Va, the rate constants in EGTA obtained for chick myosin Va were similar to those obtained here (Fig. 8). However, they proposed that the rate-determining step in EGTA was the ADP off step for chick myosin Va (42). The difference in the two studies is due to the determination of the P_i off rate in EGTA. Although the P_i off rate was not directly determined in chick myosin Va, it was estimated from the result of single turnover experiment. They observed that the initial fast phase ($40–80$ s^{-1} at 19 μM actin) was followed by the slow phase of the rate constant of 11 s^{-1} and assigned the fast phase and the slow phase as the P_i off and ADP off rate, respectively. On the other hand, we found that the initial rapid phase (fraction of $0.1–0.2$) was followed by a large fraction of the slow phase (0.06 s^{-1}; see also Fig. 3A). Since the fraction of the initial rapid phase varies with different preparations, we think that this is due to the presence of unregulated M5aFull in the preparation. Actually, the rate constant of the rapid phase was similar to the rate constant of the major fraction in Ca^{2+}. The slow single turnover rate in EGTA (0.2 s^{-1}) was also reported by Lu *et al.* (43) while the present study was under way. Furthermore, we directly measured the P_i off rate by using the fluorescent phosphate-binding protein as a probe. The rate of P_i off was markedly decreased in EGTA (Fig. 7, *A* and *B*), and the obtained rate constant explained well the slow single turnover rate of M5aFull in EGTA. At present, we do not know the reason for the apparent contradiction, but it is possible that the difference is due to the species difference between chick and mouse.

We observed that the ADP off step is biphasic for the full-length myosin Va in both Ca^{2+} and EGTA conditions. Rosenfeld and Sweeney (41) reported previously that the ADP off rate from the unregulated double-headed actomyosin Va HMM was biphasic and concluded that the biphasic ADP off rate is due to the two-head interaction of HMM. The biphasic kinetic constants in the present study are probably due to the two-headed structure of full-length myosin Va, although we cannot exclude the possibility that the dual rates are the intrinsic property of the head, since it was reported that the single-headed unregulated S1 construct also represents the biphasic ADP off rate (44). It is also reported that the ADP release rate from one head is much faster than the rate from the other head in the inhibited form of the full-length myosin Va (42). This asymmetrical ADP

TABLE 1
Kinetic parameters of M5aFull construct

Buffer conditions were as follows: 30 mM KCl, 20 mM MOPS-KOH (pH 7.5), 2 mM MgCl$_2$, 5 mM 2-mercaptoethanol, 1 mM EGTA or 0.2 mM CaCl$_2$, at 25 °C. The approximate percentage of signal amplitude is shown in parentheses, and the predominant rate is denoted in boldface type. Error represents the S.E. ($n = 3$–10).

	EGTA	Ca^{2+}	Method
Steady state			
V_o (head^{-1} s^{-1})	0.021 ± 0.001	0.055 ± 0.003	
V_{max} (head^{-1} s^{-1})	1.69 ± 0.09	14.4 ± 0.3	
K_{ATPase} (μM)	2.6 ± 0.5	0.49 ± 0.06	
Single turnover			
Without actin (s^{-1})	0.02 (30%)	0.04	ATP
	0.003 (70%)		
With actin (s^{-1})	28 ± 4 (15%)	**22 ± 4 (75%)**	mdATP
	0.31 ± 0.05 (20%)	3.5 ± 1.9 (25%)	
	0.06 ± 0.01 (65%)		
ATP binding			
$K_1k_{+2 (app)}$ (μM^{-1} s^{-1})[a]	1.91 ± 0.04	1.80 ± 0.03	mdATP
K_1k_{+2} (μM^{-1} s^{-1})	1.6 ± 0.1	1.29 ± 0.06	Tryptophan
k_{-2} (s^{-1})	0.5 ± 0.2	0.2 ± 0.2	y intercept of mdATP binding
$K_1'k_{+2 (app)}'$ (μM^{-1} s^{-1})[a]	1.38 ± 0.02	3.1 ± 0.3	mdATP
$K_1'k_{+2}'$ (μM^{-1} s^{-1})	1.6 ± 0.4	3.4 ± 0.4	Pyrene
k_{+2}' (s^{-1})	664 ± 66	694 ± 60	Pyrene
Hydrolysis			
$k_{+3} + k_{-3}$ (s^{-1})	331 ± 35	240 ± 33	Tryptophan
k_{+3} (s^{-1})	65 ± 9	188 ± 27	Calculated as $(k_{+3} + k_{-3})B$[b]
k_{-3} (s^{-1})	266 ± 29	52 ± 11	Calculated as $k_{+3} + k_{-3} - k_{-3}$
K_3	0.24 ± 0.04	3.6 ± 1.0	Calculated as k_{+3}/k_{-3}
Phosphate release			
$k_{+4 (obs)}$ (s^{-1})	0.016 ± 0.002	0.039 ± 0.002	MDCC-PBP
$k_{+4 (obs)}$ (s^{-1})	~0.003	~0.04	Quenched flow
k_{+4} (s^{-1})	0.08 ± 0.01	0.050 ± 0.004	Calculated as $k_{+4 (obs)}/B$
	~0.015		
k_{+4}' (s^{-1})	97 ± 9 (20%)	**113 ± 7 (70%)**	MDCC-PBP
	0.70 ± 0.07 (10%)	1.1 ± 0.1 (30%)	
	0.037 ± 0.002 (70%)		
ADP binding			
k_{+5} (s^{-1})	13 ± 2 (15%)	**23 ± 1 (60%)**	mdADP
	1.5 ± 0.2 (45%)	2.9 ± 0.2 (40%)	
	0.82 ± 0.03 (40%)		
k_{-5} (μM^{-1} s^{-1})	7.7 ± 0.3 (50%)	**8.5 ± 0.6 (60%)**	Mant-ADP[c]
	0.29 ± 0.02 (50%)	0.48 ± 0.06 (40%)	
k_{+5}' (s^{-1})	4 ± 1	18 ± 2	y intercept of mdADP binding
	1.7 ± 0.2	4 ± 1	
k_{+5}' (s^{-1})	11 ± 1 (20%)	**23.3 ± 0.8 (75%)**	mdADP
	3.0 ± 0.3 (55%)	3.5 ± 0.2 (25%)	
	0.66 ± 0.06 (25%)		
k_{+5}' (s^{-1})	27 ± 3 (20%)	**26 ± 2 (50%)**	Pyrene
	3.7 ± 0.3 (45%)	4.0 ± 0.8 (20%)	
	0.8 ± 0.1 (35%)	0.56 ± 0.09 (30%)	
k_{-5}' (μM^{-1} s^{-1})	**7.5 ± 0.2 (75%)**	**8.5 ± 0.6 (75%)**	mdADP[c]
	0.48 ± 0.07 (25%)	0.8 ± 0.2 (25%)	
K_5' (μM)	**0.39 ± 0.04**	**2.7 ± 0.2**	Calculated as k_{+5}'/k_{-5}'[d]
	1.4 ± 0.2	4.6 ± 1.2	
Actin binding			
$k_{+4}'/K_{9 (obs)}$ (μM^{-1} s^{-1})	0.0048 ± 0.0008	4.4 ± 0.1	MDCC-PBP
k_{+4}'/K_9 (μM^{-1} s^{-1})	0.025 ± 0.005	5.7 ± 0.3	Calculated as $k_{+4}'/K_{9 (obs)}/B$

[a] Showed averaged rates.
[b] B (Pi-burst size) was calculated as $I_{fast}/(I_{fast} + I_{slow})$ in Fig. 6, which is assumed to be $K_3/(1 + K_3)$.
[c] Analyzed by double exponential kinetics.
[d] Calculated from mdADP experiments.

release of myosin Va is due to the reduced binding affinity for actin of one head. The biphasic kinetic constants in the present study may also be due, at least in part, to the asymmetrical binding of the two heads to actin.

Regulation of Myosin Va on the Processivity—It has been known that myosin Va moves processively on actin filaments, and this is closely correlated with the high duty ratio of actomyosin Va ATPase cycle and the cooperativity between the two heads (45). The present study revealed that the duty ratio of the actomyosin Va ATP hydrolysis cycle is markedly decreased at low Ca^{2+}. This is due to the marked decrease in the P$_i$ release rate and the significant shift in the equilibrium of the ATP

hydrolysis step toward the prehydrolysis form in the inhibited state of myosin Va.

Since the ATP binding and the following actin dissociation step are fast and the equilibrium of M·ATP-AM·ATP is favored to the dissociation, it is anticipated that the full-length myosin Va at low Ca^{2+} quickly dissociates from actin upon the binding of ATP after the power stroke. It can be predicted that the decrease in the duty ratio of myosin Va at low Ca^{2+} hampers the processive movement. Supporting this notion, quite recently, it was reported that the continuous movement of single myosin Va HMM molecules was hampered by the addition of the globular tail domain (45). While this study was being conducted, Lu
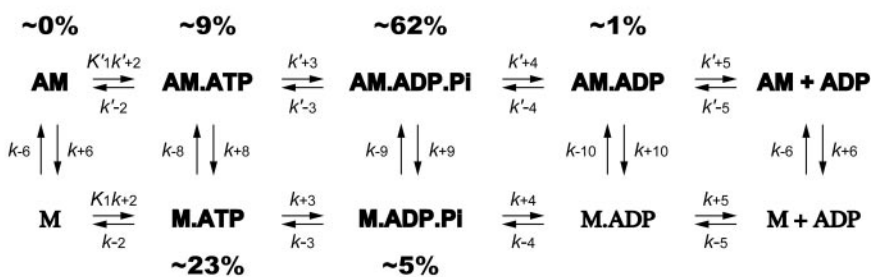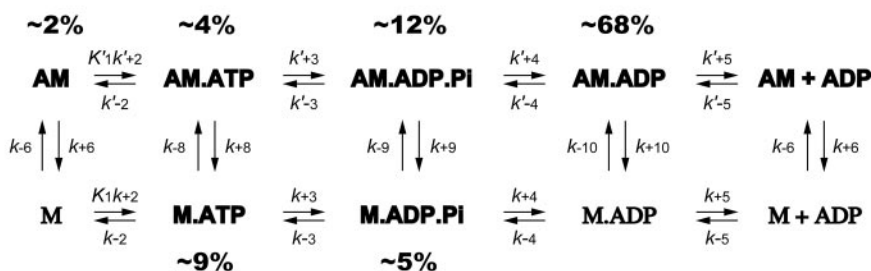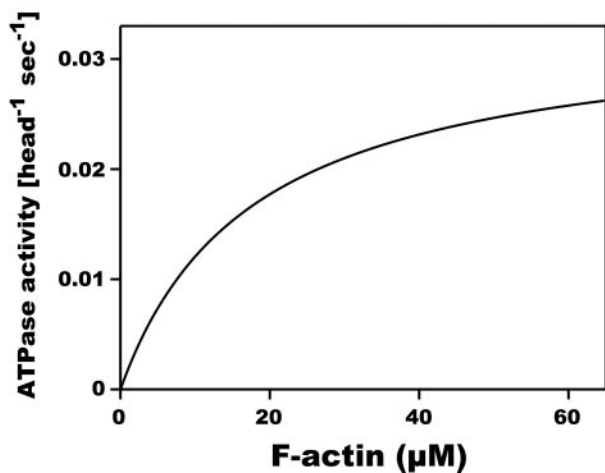
FIGURE 10. **Model of the Ca^{2+} regulation mechanism of myosin Va.** *A*, steady-state distribution of the inhibited or activated actomyosin Va intermediates. The kinetic parameters and initial values for the inhibited state were as follows: $[AM]_0 = 1$ μM, $[actin]_0 = 50$ μM, $K'_{+2} = 700$ s^{-1}, $K_8 = 100$ μM (rapid equilibrium), $k_{+3} = 65$ s^{-1}, $k_{-3} = 266$ s^{-1} ($K_3 = 0.24$), $K_9 = 4.2$ μM (rapid equilibrium), $K'_{+4} = 0.04$ s^{-1}, and $K'_{+5} = 3$ s^{-1}. The values for the active state are as follows: $[AM]_0 = 1$ μM, $[actin]_0 = 50$ μM, $K'_{+2} = 700$ s^{-1}, $K_8 = 100$ μM (rapid equilibrium), $k_{+3} = 188$ s^{-1}, $k_{-3} = 52$ s^{-1} ($K_3 = 3.6$), $K_9 = 20$ μM (rapid equilibrium), $K'_{+4} = 113$ s^{-1}, and $K'_{+5} = 20$ s^{-1}. The contribution of other equilibria to the overall scheme was ignored for simplicity of simulation. *A* and *M*, actin and myosin Va, respectively. *B*, simulated steady-state ATPase rate for the inhibited form of myosin Va. Simulation was done by varying the concentration of actin with the parameters described in the legend to *A*.

actin filaments and quickly dissociates from actin as soon as it binds to actin.

Although the molecular mechanism by which the kinetic properties are changed by Ca^{2+} is unclear, it has been proposed that the inhibition of the actin-activated ATPase activity of myosin Va at low Ca^{2+} is correlated with the large conformational change of myosin Va (16, 17, 21). It was shown that myosin Va forms a folded triangular conformation. By biochemical analysis of a series of truncated constructs, it was proposed that in the folded conformation, the head/neck domain is bent back toward the globular tail domain at the hinge between the neck and the first coiled-coil domain so that the globular tail interacts with the head of myosin Va and the C-terminal end of the coiled-coil rod (46). We showed recently that the globular tail domain functions as an intramolecular inhibitor of myosin Va, and the addition of the globular tail domain to the unregulated myosin Va HMM in EGTA produces the inhibited form of myosin Va (46). Therefore, it is expected that the processive movement of the full-length myosin Va is disrupted in the inhibited conformation.

The structural analysis revealed that the tail domain interacts with the head domain at the N-terminal lobe of the motor domain (Pro^{117}– Pro^{137}) (45) or near the nucleotide binding pocket (47). The present results are consistent with the structural findings, in which the P$_i$ and ADP release is inhibited in the folded conformation in the absence of Ca^{2+}. It is plausible that the binding of the globular tail influences the conformation of the motor domain, thus inhibiting the P$_i$ off and ADP off from the active site and the stabilization of the prehydrolysis conformation. Of interest is that the folded conformation in which the tail of myosin is bent back toward the head has also been found in conventional smooth muscle and nonmuscle myosin in the RLC dephosphorylated inhibited form (48, 49). For the conventional myosin, the P$_i$ release step is significantly inhibited in the dephosphorylated myosin to form a stable M·ADP·P$_i$ complex, and this is abolished by RLC phosphorylation at the neck. It is plausible that a common mechanism is operating for the inhibition of the product release from

et al. (43) reported that the full-length myosin Va can move processively in EGTA using single molecule imaging technique. However, the number of molecules moving processively on actin was significantly less than that in Ca^{2+}, and it is thought that the observed processive movement is due to the presence of the active form in the EGTA condition. Consistent with this notion, we found that ~10–20% of the molecules in the M5aFull preparation were unregulated (*i.e.* the active conformation). The number of molecules moved processively in EGTA was one-eighth of that in Ca^{2+} (43); therefore, it is thought that the inhibited form of myosin Va does not move on

the active site among the different myosin family members. Further studies are required to clarify the effect of the tail domain binding on the conformation of the motor domain of myosin Va.

Regulation of Myosin Va in Cells—It is not understood how the motor function of myosin Va is regulated in cells to date. However, there are at least two mechanisms for the activation of myosin Va motor function proposed. One is that Ca^{2+} binding to the CaM light chain activates the actin-activated ATPase activity (50), and the other is that the binding of the cargo molecules at the tail domain activates the ATPase activity (51). For both, a key feature is the formation of the inhibited conformation of myosin Va, which can be activated by the activation factors. The present results suggest that myosin Va in the inhibited state cannot function as a cargo transporter, because the cross-bridge cycle rate is dramatically inhibited. Furthermore, it is anticipated that myosin Va in the inhibited form dissociates from actin during the cross-bridge cycles, and it is unlikely to continuously move on actin filaments. Based upon the present results, we propose a model in which the majority of myosin Va molecules are dissociated from actin in the cells, and stimulation, such as the cargo molecule binding or the increase in Ca^{2+}, triggers myosin Va to move on actin filaments. Supporting this view, myosin Va does not show discrete colocalization with actin structure in the cells (52). Since the ATPase activity is low in the inhibited state, myosin Va consumes ATP only when it is activated and functions to transport cargos and thus minimize the energy consumption in the cells.

REFERENCES

1. Mermall, V., Post, P. L., and Mooseker, M. S. (1998) *Science* **279,** 527–533
2. Sellers, J. R. (1999) *Myosins*, 2nd Ed., Oxford University Press, New York
3. Vale, R. D. (2003) *J. Cell Biol.* **163,** 445–450
4. Mehta, A. D., Rock, R. S., Rief, M., Spudich, J. A., Mooseker, M. S., and Cheney, R. E. (1999) *Nature* **400,** 590–593
5. Rief, M., Rock, R. S., Mehta, A. D., Mooseker, M. S., Cheney, R. E., and Spudich, J. A. (2000) *Proc. Natl. Acad. Sci. U. S. A.* **97,** 9482–9486
6. Sakamoto, T., Amitani, I., Yokota, E., and Ando, T. (2000) *Biochem. Biophys. Res. Commun.* **272,** 586–590
7. Tanaka, H., Homma, K., Iwane, A. H., Katayama, E., Ikebe, R., Saito, J., Yanagida, T., and Ikebe, M. (2002) *Nature* **415,** 192–195
8. Veigel, C., Wang, F., Bartoo, M. L., Sellers, J. R., and Molloy, J. E. (2002) *Nat. Cell Biol.* **4,** 59–65
9. Langford, G. M. (2002) *Traffic* **3,** 859–865
10. Wu, X., Bowers, B., Wei, Q., Kocher, B., and Hammer, J. A., III (1997) *J. Cell Sci.* **110,** 847–859
11. Provance, D. W., Jr., Wei, M., Ipe, V., and Mercer, J. A. (1996) *Proc. Natl. Acad. Sci. U. S. A.* **93,** 14554–14558
12. Rogers, S. L., Karcher, R. L., Roland, J. T., Minin, A. A., Steffen, W., and Gelfand, V. I. (1999) *J. Cell Biol.* **146,** 1265–1276
13. Wu, X., Rao, K., Bowers, M. B., Copeland, N. G., Jenkins, N. A., and Hammer, J. A., III (2001) *J. Cell Sci.* **114,** 1091–1100
14. Lapierre, L. A., Kumar, R., Hales, C. M., Navarre, J., Bhartur, S. G., Burnette, J. O., Provance, D. W., Jr., Mercer, J. A., Bahler, M., and Goldenring, J. R. (2001) *Mol. Biol. Cell* **12,** 1843–1857
15. Rodriguez, O. C., and Cheney, R. E. (2002) *J. Cell Sci.* **115,** 991–1004
16. Li, X. D., Mabuchi, K., Ikebe, R., and Ikebe, M. (2004) *Biochem. Biophys. Res. Commun.* **315,** 538–545
17. Krementsov, D. N., Krementsova, E. B., and Trybus, K. M. (2004) *J. Cell Biol.* **164,** 877–886
18. Fukuda, M., Kuroda, T. S., and Mikoshiba, K. (2002) *J. Biol. Chem.* **277,** 12432–12436
19. Wu, X. S., Rao, K., Zhang, H., Wang, F., Sellers, J. R., Matesic, L. E., Copeland, N. G., Jenkins, N. A., and Hammer, J. A., III (2002) *Nat. Cell Biol.* **4,** 271–278
20. Strom, M., Hume, A. N., Tarafder, A. K., Barkagianni, E., and Seabra, M. C. (2002) *J. Biol. Chem.* **277,** 25423–25430
21. Wang, F., Thirumurugan, K., Stafford, W. F., Hammer, J. A., III, Knight, P. J., and Sellers, J. R. (2004) *J. Biol. Chem.* **279,** 2333–2336
22. Spudich, J. A., and Watt, S. (1971) *J. Biol. Chem.* **246,** 4866–4871
23. Kouyama, T., and Mihashi, K. (1981) *Eur. J. Biochem.* **114,** 33–38
24. Cooper, J. A., Walker, S. B., and Pollard, T. D. (1983) *J. Muscle Res. Cell Motil.* **4,** 253–262
25. White, H. D., Belknap, B., and Webb, M. R. (1997) *Biochemistry* **36,** 11828–11836
26. Brune, M., Hunter, J. L., Corrie, J. E., and Webb, M. R. (1994) *Biochemistry* **33,** 8262–8271
27. Ikebe, M., and Hartshorne, D. J. (1985) *Biochemistry* **24,** 2380–2387
28. Sato, O., White, H. D., Inoue, A., Belknap, B., Ikebe, R., and Ikebe, M. (2004) *J. Biol. Chem.* **279,** 28844–28854
29. Reynard, A. M., Hass, L. F., Jacobsen, D. D., and Boyer, P. D. (1961) *J. Biol. Chem.* **236,** 2277–2283
30. Laemmli, U. K. (1970) *Nature* **227,** 680–685
31. Hiratsuka, T. (1983) *Biochim. Biophys. Acta* **742,** 496–508
32. Houk, T. W., Jr., and Ue, K. (1974) *Anal. Biochem.* **62,** 66–74
33. De La Cruz, E. M., Wells, A. L., Rosenfeld, S. S., Ostap, E. M., and Sweeney, H. L. (1999) *Proc. Natl. Acad. Sci. U. S. A.* **96,** 13726–13731
34. De La Cruz, E. M., Sweeney, H. L., and Ostap, E. M. (2000) *Biophys. J.* **79,** 1524–1529
35. Trybus, K. M., Krementsova, E., and Freyzon, Y. (1999) *J. Biol. Chem.* **274,** 27448–27456
36. Werber, M. M., Szent-Gyorgyi, A. G., and Fasman, G. D. (1972) *Biochemistry* **11,** 2872–2883
37. Bagshaw, C. R., Eccleston, J. F., Eckstein, F., Goody, R. S., Gutfreund, H., and Trentham, D. R. (1974) *Biochem. J.* **141,** 351–364
38. De La Cruz, E. M., Wells, A. L., Sweeney, H. L., and Ostap, E. M. (2000) *Biochemistry* **39,** 14196–14202
39. Homma, K., and Ikebe, M. (2005) *J. Biol. Chem.* **280,** 29381–29391
40. Yengo, C. M., and Sweeney, H. L. (2004) *Biochemistry* **43,** 2605–2612
41. Rosenfeld, S. S., and Sweeney, H. L. (2004) *J. Biol. Chem.* **279,** 40100–40111
42. Olivares, A. O., Chang, W., Mooseker, M. S., Hackney, D. D., and De La Cruz, E. M. (2006) *J. Biol. Chem.* **281,** 31326–31336
43. Lu, H., Krementsova, E. B., and Trybus, K. M. (2006) *J. Biol. Chem.* **281,** 31987–31994
44. Hannemann, D. E., Cao, W., Olivares, A. O., Robblee, J. P., and De La Cruz, E. M. (2005) *Biochemistry* **44,** 8826–8840
45. Thirumurugan, K., Sakamoto, T., Hammer, J. A., III, Sellers, J. R., and Knight, P. J. (2006) *Nature* **442,** 212–215
46. Li, X. D., Jung, H. S., Mabuchi, K., Craig, R., and Ikebe, M. (2006) *J. Biol. Chem.* **281,** 21789–21798
47. Liu, J., Taylor, D. W., Krementsova, E. B., Trybus, K. M., and Taylor, K. A. (2006) *Nature* **442,** 208–211
48. Trybus, K. M., Huiatt, T. W., and Lowey, S. (1982) *Proc. Natl. Acad. Sci. U. S. A.* **79,** 6151–6155
49. Onishi, H., and Wakabayashi, T. (1982) *J. Biochem.* (*Tokyo*) **92,** 871–879
50. Cheney, R. E., O'Shea, M. K., Heuser, J. E., Coelho, M. V., Wolenski, J. S., Espreafico, E. M., Forscher, P., Larson, R. E., and Mooseker, M. S. (1993) *Cell* **75,** 13–23
51. Li, X. D., Ikebe, R., and Ikebe, M. (2005) *J. Biol. Chem.* **280,** 17815–17822
52. Evans, L. L., Hammer, J., and Bridgman, P. C. (1997) *J. Cell Sci.* **110,** 439–449
53. Berger, B., Wilson, D. B., Wolf, E., Tonchev, T., Milla, M., and Kim, P. S. (1995) *Proc. Natl. Acad. Sci. U. S. A.* **92,** 8259–8263